MRS Communications
© The Author(s), under exclusive licence to The Materials Research Society, 2024
https://doi.org/10.1557/s43579-024-00596-7

MRS Communications

Early Career Materials Researcher Methods Letter

A mechano-diffusion characterization platform for probing strain-programmable nanoparticle diffusion in hydrogels

Chuwei Ye, and Shaoting Lin, Department of Mechanical Engineering, Michigan State University, East Lansing, MI 48824, USA

Address all correspondence to Shaoting Lin at **linshaot@msu.edu**

(Received 1 April 2024; accepted 13 June 2024)

Abstract

Nanoparticle diffusion is a fundamental process that ubiquitously exists in life science and engineering technology. Recent studies demonstrate the potential of harnessing mechanical deformation to program nanoparticle diffusion in hydrogels, offering an expanded spectrum of nanoparticle diffusivities with precise and on-demand control. Here, we develop a mechano-diffusion characterization platform (MDCP) that integrates a mechanical system to apply controlled tension and torsion loads to deformable mediums, and an imaging system to capture spatiotemporal diffusion profiles of nanoparticles. Employing the MDCP, we study the impact of mechanical deformation on nanoparticle diffusion in hydrogels subjected to controlled stress states and loading rates.

Introduction

Nanoparticle diffusion, the movement of nanoparticles such as molecules, gold nanoparticles, and quantum dots from regions of high concentration to those of low concentration, is a fundamental phenomenon with significant implications spanning biological systems to engineering applications. On one hand, nanoparticle diffusion is pivotal in maintaining the function of living organisms as it facilitates crucial biological processes such as intracellular transport,[1,2] mucus clearance,[3] and cytoplasmic streaming.[4,5] On the other hand, advancements in technologies that manipulate nanoparticle diffusion with increased efficiency, controllability, and adaptivity revolutionize fields such as drug delivery,[6,7] chemical catalysis,[8,9] water treatment,[10,11] and electrochemical biosensing.[12,13]

Nanoparticle diffusion is typically quantified by nanoparticle diffusivity (D), which describes the rate of particles diffusing from regions of higher concentration to regions of lower concentration in a medium. Traditionally, nanoparticle diffusivity is governed by the medium viscosity, as delineated by the Stokes–Einstein equation.[14,15] However, relying solely on viscosity as the governing factor for nanoparticle diffusion presents two inherent limitations. First, viscosity lacks the necessary tunability to effectively control nanoparticle diffusion properties such as direction and speed. Second, viscosity-based nanoparticle diffusion exhibits a narrow range of nanoparticle diffusivity due to the challenge of achieving significant modifications in medium viscosity.

Our recent study exploits mechanical deformation as a new design space to program nanoparticle diffusion in hydrogels. Specifically, we develop a theoretical framework to elucidate the relationship between macroscale mechanical deformation and microscale particle diffusion. This framework reveals that the particle diffusivity is governed by three key parameters: the deformation gradient applied to the hydrogel, the normalized particle size, and a dimensionless parameter accounting for the impact of polymer network architecture.[16] In contrast to medium viscosity, employing mechanical deformation to control particle diffusion in a deformable solid medium provides inherent advantages. The first advantage is the flexibility of mechanical deformation, which allows for precise programming of particle diffusion through multi-dimensional control. For instance, by applying external loads to a deformable solid medium, particles can be directed along specific paths or assembled into desired patterns. Achieving such a level of control solely through medium viscosity is considerably challenging. The second advantage lies in the capability of mechanical deformation to facilitate real-time, on-demand manipulation and reconfiguration of particle diffusion. Unlike medium viscosity, mechanical deformations can be readily and dynamically adjusted in terms of their magnitude, direction, and timing. Despite the promising potential of strain-programmable nanoparticle diffusion, the underlying mechano-diffusion mechanism remains largely unexplored.

Methods for experimentally quantifying the spatiotemporal diffusion of nanoparticles in various mediums have been extensively developed, employing approaches through either direct visualization or indirect characterization. Direct visualization approaches are suitable for nanoparticles observable by optical systems, such as microscopes and cameras, which track nanoparticle motion followed by Brownian motion analysis. Depending on the optical system's resolution, one can measure either the concentration profile of numerous nanoparticles or the displacement of individual particles over time. For example, using a CMOS camera, one can record the spatiotemporal concentration of gold nanoparticles by detecting their visible light absorbance with a resolution of 100 μm.[17,18] Similarly, a

fluorescence microscope can capture the spatiotemporal concentration of fluorescein isothiocyanate (FITC) by monitoring its fluorescence intensity with a resolution of 1 μm.[19,20] By integrating single-particle tracking (SPT) with deep learning, diffusion characterization can be pushed to a resolution as low as 100 nm.[21] For nanoparticles that cannot be directly visualized by optical systems, indirect characterization tools such as fluorescence correlation spectroscopy (FCS),[22] dynamic light scattering (DLS),[23] and nuclear magnetic resonance (NMR)[24] can be employed to determine nanoparticle diffusivity. For example, DLS can extract nanoparticle diffusivity by measuring fluctuations in scattered light intensity associated with nanoparticle diffusion. Additionally, nanoparticle diffusivity through a membrane can be measured using a H-cell dual chamber, which measures and analyzes nanoparticle concentrations in dual chambers.[25] Compared with direct visualization approaches, indirect characterization tools or the H-cell dual chamber typically provide only the mean value of nanoparticle diffusivity in the medium. Despite existing efforts, the development of a platform for exploiting mechano-diffusion of particles in deformable medium remains largely unexplored.

Here, we develop a facile, cost-effective, and user-friendly mechano-diffusion characterization platform (MDCP), enabling systematic experimental exploration of particle diffusion characteristics in stretchable mediums under controlled stress states and tunable loading rates. The MDCP comprises a mechanical system for applying controlled tension and torsion loads to deformable mediums and an imaging system to track the spatiotemporal diffusion profiles of nanoparticles within the medium. Specifically, we utilize the MDCP to investigate the impact of mechanical deformation on the diffusion of gold nanoparticles (AuNPs) in hydrogels subjected to controlled stress states and loading rates. Our findings reveal that tension loads significantly enhance the AuNP diffusivity by 2200%, while torsion loads suppress the AuNP diffusivity by 33%. Furthermore, we observe a slightly reduced nanoparticle diffusivity under dynamic load compared to static load, possibly due to the dynamic interplay between nanoparticle hopping and chain stretching. The developed MDCP will result in a set of mechano-diffusion experimental methods and theoretical concepts, offering new insights into the mechanisms of mechano-diffusion pertinent to a broad range of biological and synthetic soft materials.

Materials and methods

For the hydrogel synthesis, a 0.5 wt% alginate acid sodium salt (Sigma-Aldrich A0682) aqueous solution was prepared, with 3 wt% acrylamide (AAm; Sigma-Aldrich A8887) used as the monomer and 0.6 wt% N, N'-methylenebisacrylamide (MBAA; Sigma-Aldrich 146072) used as crosslinker. For each 10 mL of precursor solution, 100 μL of 10 wt% ammonium persulfate (APS; Sigma-Aldrich A3678) aqueous solution was added as the thermal initiator, and 10 μL of N, N, N', N'-tetramethylethylenediamine (TEMED; Sigma-Aldrich T9281) was added as the synthesis accelerator.[17] The precursor solution was poured into a mold made from acrylic board (McMaster-Carr) and ultrathin glass slides (Corning), forming a cylindrical shape with 18 mm in diameter and 6 mm in thickness with a central hole of 2 mm in diameter and 3 mm in depth. Thereafter, the mold filled with precursor solution was placed in an incubator at 60℃ for one hour to induce free radical polymerization. To achieve axial stretch of the hydrogel sample, a glass-bonding technique was employed. Ultrathin glass slides were treated with 3-(trimethoxysilyl)propyl methacrylate (TMSPMA; Sigma-Aldrich 440159) saline solution. In 200 mL of deionized water (DI water), 50 μL of acetic acid was added, followed by an addition of 800 μL TMSPMA while stirring at 500 rpm. After 2 h of mixing, the glass slides were soaked in the solution for 3 h to create a silane-functionalized glass surface. This process ensured strong covalent bonding between the PAAm hydrogel and the glass slides during curing.[26]

Two types of AuNPs with average core diameters of 6 nm and 18 nm were synthesized in this work. For the synthesis of 6 nm AuNPs, gold (III) chloride trihydrate ($HAuCl_4 \cdot 3H_2O$; Sigma-Aldrich 520918) was used, with tri-sodium citrate (Sigma-Aldrich S1804) serving as the stabilization agent and sodium borohydride ($NaBH_4$; Sigma-Aldrich 452882) as the reducing agent.[27] Specifically, 20 mL of 0.25 mM $HAuCl_4$ and 0.25 mM tri-sodium citrate aqueous solution was prepared. Under stirring at 650 rpm, 600 μL ice-cold 0.1 M $NaBH_4$ solution was slowly added into the mixture, which instantly transforms the colorless solution into ruby red, indicating the formation of 6 nm AuNPs. The AuNPs solution was stabilized for 1 h to ensure a thorough reaction. For the synthesis of 18 nm AuNPs, 20 mL of 0.25 mM $HAuCl_4$ solution was heated to boiling under stirring at 650 rpm, and 2 mL of 1 wt% tri-sodium citrate aqueous solution was slowly added. Initially, the solution turns a light purple color and then bright ruby red upon continuous boiling, indicating the formation of 18 nm AuNPs. Thereafter, boiling was continued for 10 min to complete the reaction, followed by a 1-h cooling period to stabilize the solution. To functionalize the AuNPs with PEG chains rendering their surfaces inert and neutrally charged, a 1 kDa PEG chain with a thiol head group (MPEG1000-SH; Nanosoft Biotechnology SKU 2514-1000) solution was prepared. Specifically, 500 mg of MPEG1000-SH was added to 500 μL of DI water, mixed, and then added to the 20 mL stabilized AuNPs solution under stirring at 650 rpm.[17] The PEG-capped AuNPs solution presenting a deeper red color was mixed for 1 h.

The core diameter and hydrodynamic diameter of the AuNPs were characterized by transmission electron microscopy (TEM) and dynamic light scattering (DLS), respectively. TEM imaging was performed using the JEOL 1400 Flash TEM equipment, which operates at a maximum accelerating voltage of 120 kV and provides a lattice resolution of 0.2 nm. DLS measurements were conducted using the Malvern Zetasizer Nano-ZS equipment. Diffusion profile images were captured every 30 min by an SVPRO Web Camera at a resolution of 3264 pixels × 2448 pixels. These images were converted into grayscales using

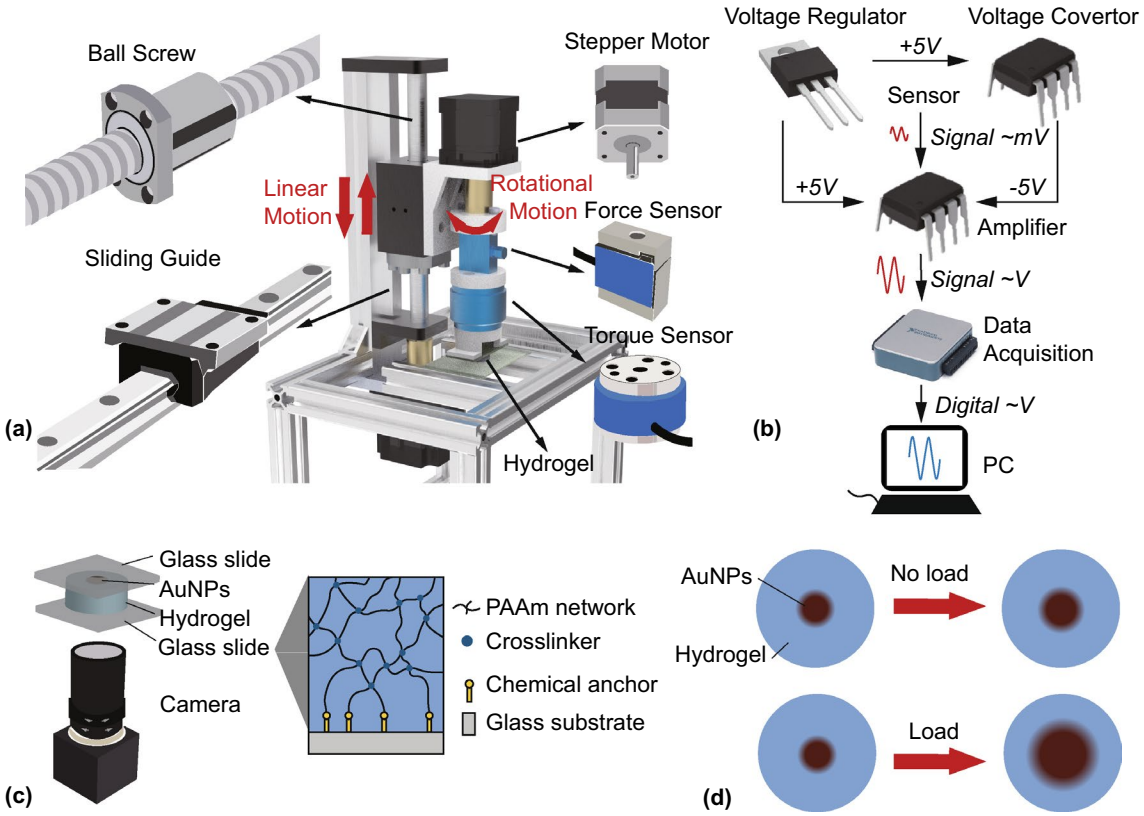


Figure 1. Design of the mechano-diffusion characterization platform (MDCP). (a) The mechanical loading system for linear and rotational actuations. (b) The electronic system for signal amplification and data acquisition. (c) The imaging system captures the diffusion profiles of the AuNPs in the hydrogel bonded to the glass substrates. (d) The schematics comparing the diffusion profiles of AuNPs in hydrogels with and without load.

MATLAB software, and the grayscale values were normalized from 0 to 1 to represent the normalized concentration of AuNPs in the hydrogel.

Results and discussions

Design of MDCP

For the mechanical loading system, a two-phase stepper motor drives a 1604-type ball screw to achieve linear actuation, while another two-phase stepper motor provides rotational actuation. An Arduino UNO serves as the microcontroller to control the motion of both stepper motors. Force measurement is accomplished using a load cell with a 9.8 N range and a 1.9 mV/V sensitivity, while torque measurement is achieved by a torque sensor with a 0.3 N·m range and a 0.6 mV/V sensitivity [Fig. 1(a)]. To process the measurement data, an electronic amplification system is constructed. Since the sensor outputs are in millivolts, an INA128P instrumentation amplifier is applied,[28] powered by a ±5 V power supply generated from an LM7805 voltage regulator and a MAX660 voltage converter,[29,30] boosting the output voltage to volt levels. The amplified data is then fed into the NI USB6008 data acquisition device, which connects to a personal computer for display, recording, and analysis [Fig. 1(b)].[31] As shown in Fig. 2 and the supplementary videos 1 and 2, the mechanical loading system can simultaneously apply and record controlled tension and torsion loads on silicon rubber. By applying cyclic tensile loads, the silicon rubber undergoes shape variations, allowing the calculation of nominal stress based on the force measured by the tensile sensor [Fig. 2(a)]. Additionally, the system demonstrates its capability to impose cyclic torsion loads on the silicon rubber, with the torque monitored by the embedded torque sensor [Fig. 2(b)]. Continuous adjustment of the linear and angular velocities of the loading system enables the application of various loading rates to hydrogel samples in subsequent diffusion experiments.

A high-resolution camera with a maximum resolution of 3264 pixels × 2448 pixels and a video capture capability of 15 frames per second is employed to capture images, depicting the diffusion profiles of the AuNPs in the hydrogel. In the experiments, the camera resolution is approximately 0.015 mm/pixel, which is adequate for determining the diffusivity, as the diffusion profiles are on the millimeter scale. By applying the glass-bonding technique,[26] the PAAm hydrogel is robustly bonded to the glass slides, allowing the application of tension and torsion loads on the hydrogel samples by manipulating the glass slides [Figs. 1(c), S8]. Analyzing the spatiotemporal diffusion

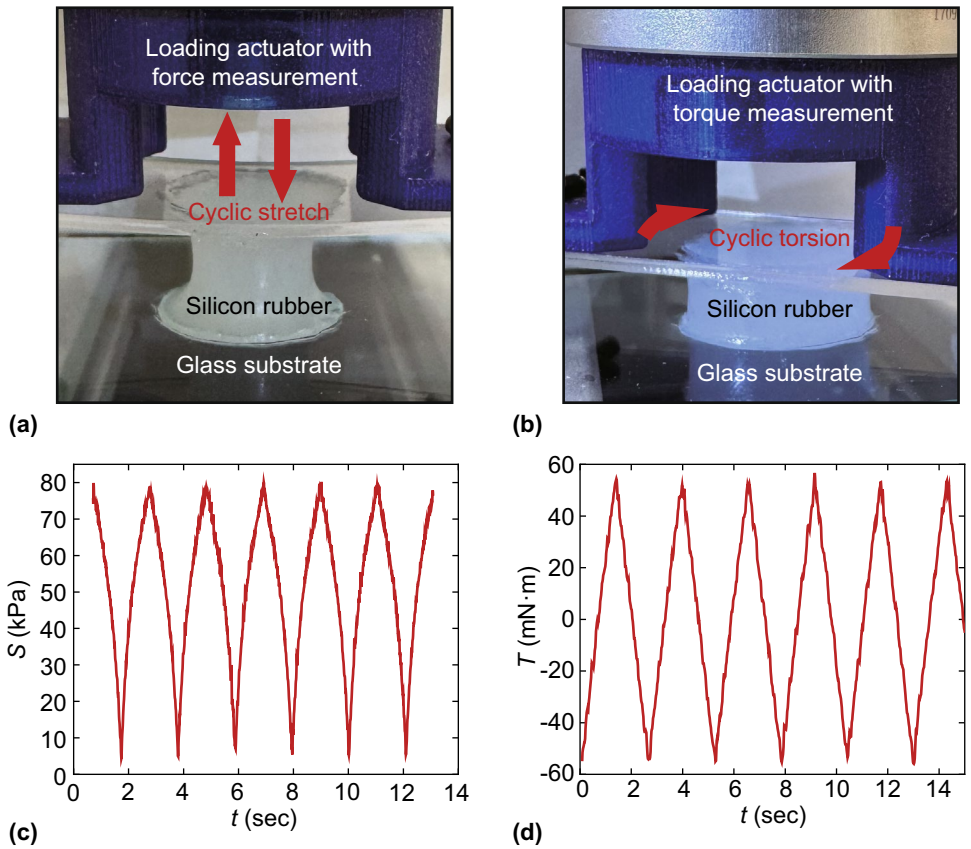


Figure 2. Capability of MDCP in force and torque measurements. (a) The optical image of the loading platform applying cyclic stretch to the silicon rubber sample. (b) The optical image of the loading platform applying cyclic torsion to the silicon rubber sample. (c) The measured nominal stress *S* as a function of time based on the recorded force. (d) The measured torque *T* as a function of time.

profiles enables the study of the effect of mechanical deformation on AuNP diffusivity in hydrogels under controlled stress states and loading rates [Fig. 1(d)]. In future work, we plan to adopt an imaging system with extremely high resolution, near 10 nm, to track the dynamics of individual particle diffusion in the hydrogel using single-particle tracking techniques.[32]

Characterization of AuNPs and hydrogels

AuNPs are surface modified with shells composed of 1 kDa PEG chains, resulting in inert surfaces. This modification features the AuNPs' dimensions in terms of the core diameter d_c and the hydrodynamic diameter d_h, representing the core of pure AuNPs and the overall AuNPs with PEG shells, respectively [Fig. 3(a)]. Transmission electron microscopy (TEM) is used to determine the mean core diameter, which measures 6 nm and 18 nm for the two types of synthesized AuNPs, respectively [Fig. 3(b), Fig. S1]. Dynamic light scattering (DLS) measures the hydrodynamic diameters of 12 nm and 28 nm for the two types of synthesized AuNPs, respectively [Fig. 3(c)].

To further characterize the mechanical properties of the PAAm hydrogel, we fabricate dog-bone-shaped samples of the hydrogel following the ASME standard. We first perform single-cycle uniaxial tensile experiments to characterize the mechanical dissipation of the PAAm hydrogel under nonlinear large deformation. As shown in Fig. 3(d), the PAAm hydrogel exhibits negligible mechanical hysteresis in the stress-stretch curve, indicating negligible mechanical dissipation. Next, we perform multiple-cycle uniaxial tensile experiments to characterize the fatigue response of the PAAm hydrogel. Specifically, the dog-bone-shaped sample is subjected to 1000 cycles of stretch-recovery loading, with a maximum stretch ratio of $\lambda_{max}=2.0$. As shown in Fig. 3(e), there is negligible shake-down in the stress-stretch curve after the 1000-cycle loading–unloading process, indicating that the PAAm hydrogel experiences little fatigue-induced damage.

Spatiotemporal diffusion characterization of AuNPs in hydrogels

A typical diffusion profile sequence of AuNPs diffusing in the hydrogel sample is presented in Fig. 3(f). Initially, the AuNPs solution is placed in the central hole of the hydrogel sample. When a tensile load is applied to the sample, the AuNPs diffuse radially, forming an increasingly larger circle of AuNPs. The total observation time is 150 min. During the experiments, tension or torsion is applied to the hydrogel, the AuNPs are

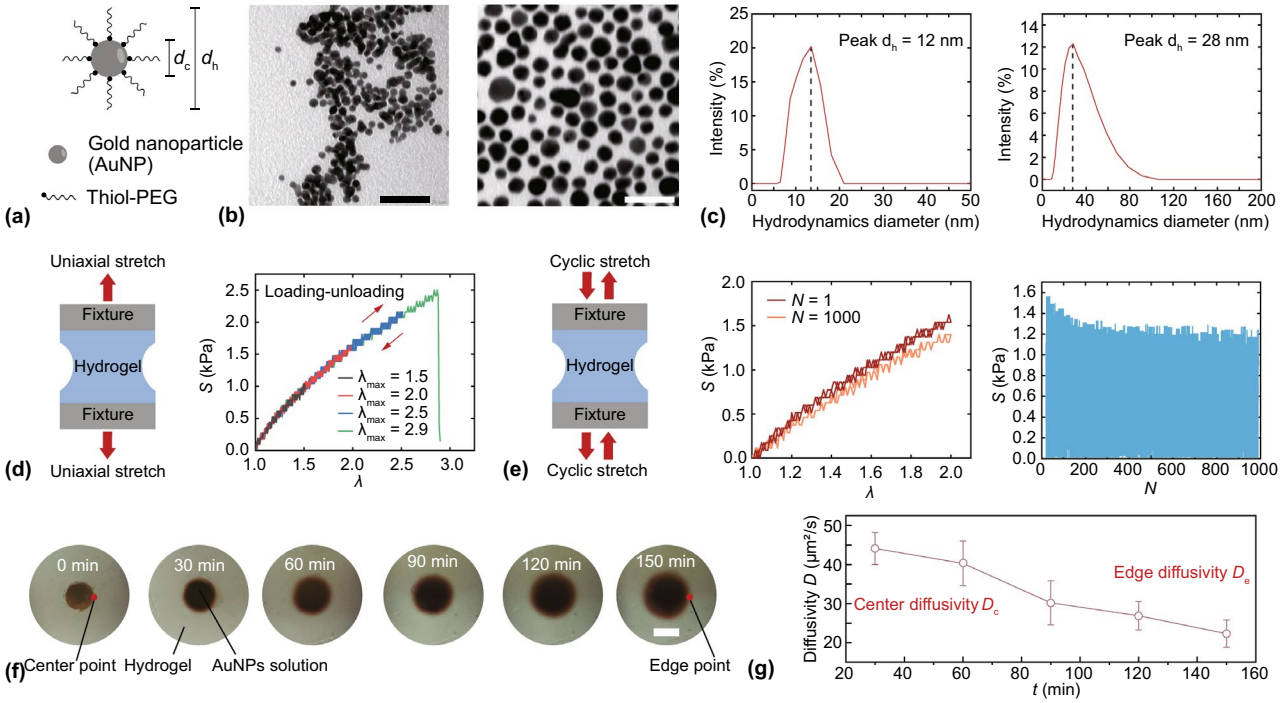


Figure 3. Mechanical, structural, and diffusion characterizations of the AuNP-hydrogel system. (a) Schematic illustration of the AuNPs capped with PEG polymer chains with the core diameter as d_c and the hydrodynamic diameter as d_h. (b) TEM images of two types of AuNPs showing mean core diameters as 6 nm and 18 nm. (c) DLS measurements of two types of AuNPs measuring hydrodynamic diameters as 12 nm and 28 nm. (d) Nominal stress versus stretch curve of the hydrogel under a single cycle of loading and unloading. (e) Nominal stress versus stretch curve of the hydrogel under multiple cycles of loading and unloading. (f) The profiles of the AuNPs diffusion in hydrogel medium. (g) Measured diffusivity as a function of time, with short-term diffusivity corresponding to the center diffusivity D_c and long-term diffusivity corresponding to the edge diffusivity D_e. The scale bars in (b) and (f) are 50 nm and 2 mm, respectively. Values in (g) represent the mean and standard deviation ($n = 3$).

allowed to diffuse for 30-min intervals while the hydrogel is deformed. After each interval, the deformation is released, and images of the diffusion profiles are captured in the undeformed state, ensuring the hydrogel sample's dimensions remain unchanged when evaluating diffusivity.

To extract the diffusivity, we use the numerical finite difference method (FDM) implemented in MATLAB to solve the diffusion governing equation in the cylindrical coordinate system. We first use MATLAB to obtain grayscale values from the captured images of the diffusion profile, where the intensity of the grayscale value represents the concentration of the AuNPs. Thereafter, we fit the governing diffusion equation to these experimentally extracted grayscale values to determine the diffusivity. The governing diffusion equation in the Cartesian coordinate system is as follows:

$$\frac{\partial c}{\partial t} = D\frac{\partial^2 c}{\partial x^2} \tag{1}$$

where c is concentration, t is diffusion time, x is diffusion distance, and D is diffusivity. In the cylindrical coordinate system, Eq. 1 can be further expressed as:

$$\frac{\partial c}{\partial t} = D\left(\frac{1}{r}\frac{\partial}{\partial r}\left(r\frac{\partial c}{\partial r}\right) + \frac{1}{r^2}\frac{\partial^2 c}{\partial \theta^2} + \frac{\partial^2 c}{\partial z^2}\right) \tag{2}$$

where r is the diffusion distance along radial direction, z is the axial distance, θ is the angular coordinate. Since the diffusion is symmetrical in the angular direction, namely $\partial c/\partial\theta = 0$, the Eq. 2 can be further simplified as:

$$\frac{\partial c}{\partial t} = D\left(\frac{1}{r}\frac{\partial}{\partial r}\left(r\frac{\partial c}{\partial r}\right) + \frac{\partial^2 c}{\partial z^2}\right) = D\left(\frac{\partial^2 c}{\partial r^2} + \frac{1}{r}\frac{\partial c}{\partial r} + \frac{\partial^2 c}{\partial z^2}\right) \tag{3}$$

In this study, the cylindrical sample occupies the domain where $-9 < r < 9$ and $0 < z < 6$ in millimeters (mm) as illustrated in Fig. S2. The concentration of AuNPs in the reservoir that occupies the domain where $-1.5 < r < 1.5$ and $3 < z < 6$ is set as a constant $c = c_0$; and the initial concentration in the rest of the sample is set as $c = 0$. We use finite difference methods in MATLAB to numerically solve Eq. 3. By fitting the simulated concentration profile to the measured concentration profile, we can determine the measured diffusivity D as summarized in Figs. S3–S6.

Traditionally, nanoparticle diffusivity is considered constant throughout the diffusion process.[33] However, in our experiments, we observe that the diffusivity of AuNPs is spatially dependent due to the nonuniform stress distribution. Specifically, the diffusivity decreases as the nanoparticles diffuse from the center to the edge of the sample. We attribute

this spatial dependency to the strain-dependent nature of nanoparticle diffusivity in deformed hydrogels, which results from nonuniform strain distributions within the cylindrical hydrogel samples.[34] Generally, the impact of mechanical deformation on nanoparticle diffusion is governed by two competing effects according to our recent study:[16] (1) a decreased energy barrier that promotes particle diffusivity, and (2) a distorted mesh size that hinders particle diffusivity. To quantify this phenomenon, we take the measured nanoparticle diffusivity at the center of the sample as center diffusivity D_c, while defining the measured nanoparticle diffusivity at the edge of the sample as edge diffusivity D_e. As shown in Fig. 3(g), the center diffusivity D_c is higher than the edge diffusivity D_e.

Impact of loading rates and stress states on AuNP diffusivity

To systematically investigate the impacts of mechanical deformation on the diffusivity of AuNPs in hydrogels under controlled stress states and loading rates, we conduct comparative experiments, using our MDCP characterization platform to apply controlled tension and torsion loads at various stretching rates and torsion angles [Fig. 4(a)].

We first conduct comparative experiments between AuNPs with core diameters of 6 nm and 18 nm in the hydrogel sample under static tensile load. As shown in Fig. 4(b), AuNPs with $d_c = 6$ nm exhibit more pronounced spatial-dependent nanoparticle diffusivity compared to AuNPs with $d_c = 18$ nm. As shown in Fig. 4(b), the center diffusivity of AuNPs with $d_c = 6$ nm exceeds 68 μm^2/s, which is significantly higher than that of AuNPs with $d_c = 18$ nm around 44 μm^2/s. This discrepancy is mainly attributed to the difference in AuNP diameters in that larger AuNPs overcome higher energy barriers compared to smaller ones.[35,36]

We further conduct comparative experiments between AuNPs with core diameters of 6 nm and 18 nm in the hydrogel sample under dynamic tensile load. Consistently, the center diffusivity is higher than the edge diffusivity for both AuNPs, with the diffusivity of AuNPs with $d_c = 6$ nm being higher than that of AuNPs with $d_c = 18$ nm [Fig. 4(c)]. Notably, the diffusivity under dynamic tensile load is lower than that under static load. This reduction in diffusivity can be attributed to the interplay between the time for particles hopping and the duration of the loading–unloading cycle. The shorter recovery time for the hydrogel polymer networks from the deformed state results in a shorter responsive time for particles to hop through, leading to lower diffusivity. To further validate this assumption, we conduct experiments to evaluate the relaxation time of the polymer networks. As described in Fig. S7, the relaxation time is 19.4 s, much longer than our loading–unloading cycle period of 2 s. Therefore, the rapid loading rate is sufficient to influence the hopping diffusion process in the hydrogel.

The loading rate modulates the mode of diffusion, depending on the interplay among three critical time scales: the time

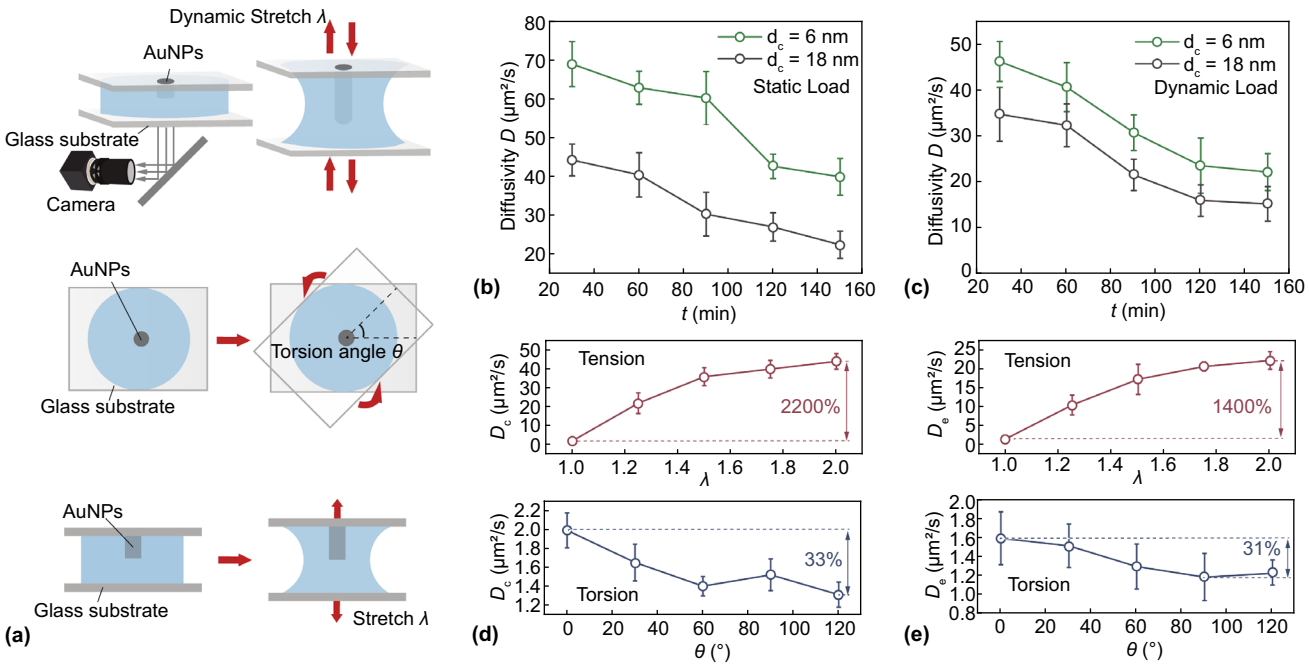


Figure 4. Mechano-diffusion characterizations of AuNPs in hydrogels under various conditions. (a) Schematic illustration of mechano-diffusion characterizations of AuNPs in hydrogels subjected to tension and torsion under static and dynamic loads. (b) Diffusivity D as a function of time t for the two types of AuNPs in hydrogels subjected to static tension $\lambda = 2$. (c) Diffusivity D as a function of time t for the two types of AuNPs in hydrogels subjected to dynamic tension $\lambda = 2$ at a stretch rate of 2 s^{-1}. (d) The comparison of center diffusivities D_c of AuNPs with $d_c = 18$ nm in hydrogels under static tension and static torsion. (e) The comparison of edge diffusivities D_e of AuNPs with $d_c = 18$ nm in hydrogels under static tension and static torsion. Values in (b-f) represent the mean and standard deviation ($n = 3$).

scale associated with the loading rate τ_1, the time scale for the relaxation of the polymer chains τ_2, and the time scale for particle diffusion τ_3. At a low loading rate ($\tau_1 \gg \tau_2, \tau_3$), the diffusion system has sufficient time to reach equilibrium, and the diffusion process is primarily governed by the inherent particle diffusivity D without interference from loading rate. At a high loading rate ($\tau_1 \ll \tau_2, \tau_3$), the polymer chains do not have enough time to relax during loading, leading to a non-equilibrium state where polymer chain relaxation and particle hopping diffusion are coupled. Our experiments show that particles in a dynamically stretched hydrogel exhibit reduced diffusivity due to this non-equilibrium hopping diffusion process.[37]

We also perform comparative experiments for hydrogel samples under tension and torsion loads. First, we investigate the center diffusivity of AuNPs in hydrogel samples under static tension and torsion loads. The stretch ratios of the hydrogel samples range from 1.0 to 2.0, while the torsion angles range from 30 to 120 degrees. We observe the diffusivity of the AuNPs in hydrogels under tension is much higher than that in hydrogels under torsion. Specifically, our experimental results show that tension loads significantly enhance the center diffusivity of AuNPs by 2200%, while torsion loads suppress the center diffusivity of AuNPs by 33% [Fig. 4(d)]. Next, we investigate the edge diffusivity of the AuNPs in the samples. The trend in edge diffusivity mirrors that of the center diffusivity: tensile load promotes diffusion, whereas torsion load inhibits diffusion [Fig. 4(e)]. The reduction of diffusivity in hydrogels under torsion can be attributed to the distortion of polymer mesh and the reduction of the mesh size, increasing the energy barrier for AuNPs hopping and consequently leading to lower diffusivity. In hydrogels under tension, the decreased energy barrier predominates, leading to significantly enhanced particle diffusivity. In contrast, in hydrogels under torsion, near the center of the sample where deformation is minimal, the distorted mesh size predominates, suppressing particle diffusivity.

Conclusions

In this work, we develop a characterization platform, MDCP, designed for studying the mechano-transport of AuNPs in hydrogels under controlled stress states and loading rates. This platform, which is both user-friendly and cost-effective, proves highly effective for observing and analyzing diffusion processes under mechanical loading. To validate its functionality, we synthesize a hydrogel with no hysteresis loop in its stress-stretch curve as the diffusion medium, and two kinds of AuNPs with different core and hydrodynamic diameters as the diffusing nanoparticles. We conduct a series of comparative experiments, including tests with different particle sizes in hydrogels under identical stress states, investigations of the diffusion of AuNPs in the hydrogel medium under various loading rates, and comparisons of diffusivity between tension and torsion loads. By analyzing the results of the mechano-transport experiments, we can conclude that: (1) Larger particle sizes correspond to lower diffusivity; (2) Dynamic loads suppress the diffusion of AuNPs in hydrogels under tension; (3) Tension loads promote the diffusion of AuNPs, while the torsion load inhibits it. In summary, our MDCP offers a novel method for studying particle diffusion in stretchable media, such as polymeric hydrogels, under various stress states by applying different loads. Additionally, it quantifies the trends in diffusivity variations in non-equilibrium states of the diffusion medium.

In future work, this platform can be extended to study the behavior of various types of nanoparticles with different shapes and surface properties. For instance, the surface properties of particles introduce an additional design space, enabling selective diffusion design in hydrogels. Different affinities between the particles and the polymer networks can result in three modes of selective diffusion: Brownian diffusion, arrested diffusion, and walking diffusion. Combined with mechanical deformation, the MDCP can further serve as a platform to explore the potential for achieving strain-programmable active selective transport in hydrogels.[18,38]

Acknowledgments

We thank Alicia Withrow for help with transmission electron microscopy imaging and Wei Zhang and Romilly Benedict for help with the dynamic light scattering characterization.

Author contributions

CY: Methodology, Data acquisition, Writing-original draft. SL: Conceptualization, Supervision, Writing-review and editing.

Funding

This research was funded by NSF-CBET-2320716.

Data availability

Data will be made available on reasonable request.

Declarations

Conflict of interest

The authors declare that they have no conflict of interest.

Supplementary Information

The online version contains supplementary material available at https://doi.org/10.1557/s43579-024-00596-7.

References

1. S. Patel et al., Naturally-occurring cholesterol analogues in lipid nanoparticles induce polymorphic shape and enhance intracellular delivery of mRNA. Nat. Commun. **11**, 983 (2020). https://doi.org/10.1038/s41467-020-14527-2
2. M. Liu et al., Real-time visualization of clustering and intracellular transport of gold nanoparticles by correlative imaging. Nat. Commun. **8**, 15646 (2017). https://doi.org/10.1038/ncomms15646

3. M.I. Pino-Argumedo et al., Elastic mucus strands impair mucociliary clearance in cystic fibrosis pigs. Proc. Natl. Acad. Sci. U.S.A. **119**, e2121731119 (2022). https://doi.org/10.1073/pnas.2121731119
4. H. Gu et al., Artificial microtubules for rapid and collective transport of magnetic microcargoes. Nat. Mach. Intell. **4**, 678–684 (2022). https://doi.org/10.1038/s42256-022-00510-7
5. A. Mateu-Regue et al., Single mRNP analysis reveals that small cytoplasmic mRNP granules represent mRNA singletons. Cell Rep. **29**, 736–748 (2019). https://doi.org/10.1016/j.celrep.2019.09.018
6. S. Hu et al., A mussel-inspired film for adhesion to wet buccal tissue and efficient buccal drug delivery. Nat. Commun. **12**, 1689 (2021). https://doi.org/10.1038/s41467-021-21989-5
7. S. Basu et al., Numerical evaluation of spray position for improved nasal drug delivery. Sci. Rep. **10**, 10568 (2020). https://doi.org/10.1038/s41598-020-66716-0
8. H.S. Muddana, S. Sengupta, T.E. Mallouk, A. Sen, P.J. Butler, Substrate catalysis enhances single-enzyme diffusion. J. Am. Chem. Soc. **132**, 2110–2111 (2010)
9. Y. Qin et al., Hollow mesoporous metal–organic frameworks with enhanced diffusion for highly efficient catalysis. ACS Catal. **10**, 5973–5978 (2020)
10. S. Raju et al., Improved methodology to determine the fate and transport of microplastics in a secondary wastewater treatment plant. Water Res. **173**, 115549 (2020). https://doi.org/10.1016/j.watres.2020.115549
11. S. Freeman et al., Between source and sea: the role of wastewater treatment in reducing marine microplastics. J. Environ. Manage. **266**, 110642 (2020). https://doi.org/10.1016/j.jenvman.2020.110642
12. H. Zhang et al., In situ formation of gold nanoparticles decorated Ti3C2 MXenes nanoprobe for highly sensitive electrogenerated chemiluminescence detection of exosomes and their surface proteins. Anal. Chem. **92**, 5546–5553 (2020)
13. S. Lin et al., Natural perspiration sampling and in situ electrochemical analysis with hydrogel micropatches for user-identifiable and wireless chemo/biosensing. ACS Sens. **5**, 93–102 (2020). https://doi.org/10.1021/acssensors.9b01727
14. C.C. Miller, The Stokes–Einstein law for diffusion in solution. Proc. R. Soc. London Ser. A, Containing Papers Math. Phys. Charact. **106**, 724–749 (1924)
15. Q. Liu, S. Huang, Z. Suo, Brownian motion of molecular probes in supercooled liquids. Phys. Rev. Lett. **114**, 224301 (2015). https://doi.org/10.1103/PhysRevLett.114.224301
16. J. Liu, S. Lin, Strain-engineered particle diffusion in uniaxially deformed polymer networks. J. Mechan. Phys. Solids (2024). https://doi.org/10.1016/j.jmps.2024.105732
17. P.J. Moncure, Z.C. Simon, J.E. Millstone, J.E. Laaser, Relationship between gel mesh and particle size in determining nanoparticle diffusion in hydrogel nanocomposites. J. Phys. Chem. B **126**, 4132–4142 (2022). https://doi.org/10.1021/acs.jpcb.2c00771
18. Y. Gu, M.E. Distler, H.F. Cheng, C. Huang, C.A. Mirkin, A general DNA-gated hydrogel strategy for selective transport of chemical and biological cargos. J. Am. Chem. Soc. **143**, 17200–17208 (2021)
19. J. Floury, M.-N. Madec, F. Waharte, S. Jeanson, S. Lortal, First assessment of diffusion coefficients in model cheese by fluorescence recovery after photobleaching (FRAP). Food Chem. **133**, 551–556 (2012)
20. Y.G. Anissimov, X. Zhao, M.S. Roberts, A.V. Zvyagin, Fluorescence recovery after photo-bleaching as a method to determine local diffusion coefficient in the stratum corneum. Int. J. Pharm. **435**, 93–97 (2012)
21. H.H. Park, B. Wang, S. Moon, T. Jepson, K. Xu, Machine-learning-powered extraction of molecular diffusivity from single-molecule images for super-resolution mapping. Commun. Biol. **6**, 336 (2023)
22. A.B. Andrews, R.E. Guerra, O.C. Mullins, P.N. Sen, Diffusivity of asphaltene molecules by fluorescence correlation spectroscopy. J. Phys. Chem. A **110**, 8093–8097 (2006)
23. R. Pecora, Dynamic light scattering measurement of nanometer particles in liquids. J. Nanopart. Res. **2**, 123–131 (2000)
24. G. Costantini, S. Capuani, F.A. Farrelly, A. Taloni, A new perspective of molecular diffusion by nuclear magnetic resonance. Sci. Rep. **13**, 1703 (2023)
25. A.J. Grodzinsky, *Fields, forces, and flows in biological systems* (CRC Press, Boca Raton, 2011)
26. H. Yuk, T. Zhang, S. Lin, G.A. Parada, X. Zhao, Tough bonding of hydrogels to diverse non-porous surfaces. Nat. Mater. **15**, 190–196 (2016)
27. A. Gole, C.J. Murphy, Seed-mediated synthesis of gold nanorods: role of the size and nature of the seed. Chem. Mater. **16**, 3633–3640 (2004)
28. Kafadar, Ö. & Sondaş, A. in *2016 20th National Biomedical Engineering Meeting (BIYOMUT).* 1–4 (IEEE).
29. M. Divya, K. Saravanan, G.N. Balaji, S.C. Pandian, Light weight & low cost power bank based on LM7805 regulator for hand held applications. Int. J. Latest Technol. Eng. Manage. Appl. Sci. (IJLTEMAS) **7**, 201–205 (2018)
30. Brooks, R. A. *An electronic compass for small autonomous robots*, Citeseer, (1993)
31. C. Bharatiraja, J. Munda, I. Vaghasia, R. Valiveti, P. Manasa, Low cost real time centralized speed control of DC motor using lab view-NI USB 6008. Int. J. Power Electron. Drive Syst. **3**, 656–664 (2016)
32. Z. Sun, J. Fan, H. Li, H. Jiang, Current status of single particle imaging with X-ray lasers. Appl. Sci. **8**, 132 (2018)
33. P.J. Moncure, Z.C. Simon, J.E. Millstone, J.E. Laaser, Relationship between gel mesh and particle size in determining nanoparticle diffusion in hydrogel nanocomposites. J. Phys. Chem. B **126**, 4132–4142 (2022)
34. S. Lin, Y. Mao, R. Radovitzky, X. Zhao, Instabilities in confined elastic layers under tension: fringe, fingering and cavitation. J. Mech. Phys. Solids **106**, 229–256 (2017)
35. S.H. Kim et al., The effect of ζ-potential and hydrodynamic size on nanoparticle interactions in hydrogels. Part. Part. Syst. Charact. **36**, 1800292 (2019)
36. L.H. Cai, S. Panyukov, M. Rubinstein, Hopping diffusion of nanoparticles in polymer matrices. Macromolecules **48**, 847–862 (2015). https://doi.org/10.1021/ma501608x
37. Michael Rubinstein, R. H. C. *Polymer Physics*. (2003)
38. Y.J. Yang, D.J. Mai, S. Li, M.A. Morris, B.D. Olsen, Tuning selective transport of biomolecules through site-mutated nucleoporin-like protein (NLP) hydrogels. Biomacromol **22**, 289–298 (2021)

Publisher's Note Springer Nature remains neutral with regard to jurisdictional claims in published maps and institutional affiliations.

Springer Nature or its licensor (e.g. a society or other partner) holds exclusive rights to this article under a publishing agreement with the author(s) or other rightsholder(s); author self-archiving of the accepted manuscript version of this article is solely governed by the terms of such publishing agreement and applicable law.